Journal of Alloys and Compounds 722 (2017) 438–444

Contents lists available at ScienceDirect

Journal of Alloys and Compounds

journal homepage: http://www.elsevier.com/locate/jalcom

Novel borate $CsZn_2B_3O_7$ single crystal with large efficient second harmonic generation in deep-ultraviolet spectral range

A.H. Reshak [a, b, *]

[a] New Technologies - Research Centre, University of West Bohemia, Univerzitni 8, 306 14 Pilsen, Czech Republic
[b] School of Material Engineering, University Malaysia Perlis, 01007 Kangar, Perlis, Malaysia

ARTICLE INFO

Article history:
Received 28 April 2017
Received in revised form
6 June 2017
Accepted 11 June 2017
Available online 12 June 2017

Keywords:
Second harmonic generation
Deep-ultraviolet
$CsZn_2B_3O_7$ single crystal

ABSTRACT

The linear and nonlinear optical susceptibility dispersion of $CsZn_2B_3O_7$ single crystal are comprehensively investigated for a bulk structure in form of single crystal taking into account the influence of the packing structural units. The calculation highlights that the BO_3 structural units packing is the main source for the large birefringence in $CsZn_2B_3O_7$ due to high anisotropic electron distribution, and, hence, it affects the macroscopic second harmonic generation (SHG) coefficients. The large SHG is due to hyperpolarizablity formed by ZnO_4 tetrahedra and co-parallel BO_3 triangle groups. The absorption edge of $CsZn_2B_3O_7$ occurs at $\lambda = 218$ nm and the optical band gap is estimated to be 5.68 eV that is in good agreement with the experimental data (5.69 eV). Therefore, $CsZn_2B_3O_7$ is expected to produce a coherent radiation in deep-ultraviolet (DUV) region with SHG of about 1.5 × KDP (1.5 × 0.39 p.m./V = 0.585 p.m./V) that agrees with the measurements. This work is aimed at the report of reliable SHG value and the details of the NLO tensor for bulk $CsZn_2B_3O_7$ single crystal.

© 2017 Elsevier B.V. All rights reserved.

1. Introduction

Since the first observation of second harmonic generation (SHG) phenomenon [1], nonlinear optics are of great interest and attracted tremendous attention of the workers in laser science and technology. The nonlinear optical (NLO) materials are among the most important types of optoelectronic functional materials which are widely used in optical frequency conversion [2–7]. The NLO materials are very essential due to their ability to produce light at wavelengths which are inaccessible via conventional sources; for instance ultraviolet (UV) and deep-ultraviolet (DUV) laser radiation [8–11]. The search for novel NLO materials with promising structural and optical properties is still a challenge for scientists. To produce a radiation in UV and DVU regions, the NLO material should possesses wide energy band gap i.e. short absorption cutoff, relatively high birefringence and the refractive indices dispersion in the UV and DUV regions must be small enough to match the fundamental wave with the SHG light [12]. However, efficient design of a suitable high-performing NLO material remains challenging. It was reported that in borate materials, the large electronegativity difference between B and O atoms is very favorable for transmittance of short-wavelength light [13]. In general, the B and O atoms in borates forms planer triangles $(BO_3)^{3-}$ and $(BO_4)^{5-}$ polyhedra. The BO_3 groups can adopt a coplanar configuration promoting birefringence and SHG. In BO_3 groups, three O atoms are linked with B atom, eliminating three dangling bonds of the BO_3 groups, which further widens its transparence in the UV and DUV region. Moreover, the highly anisotropic electron distribution in BO_3 group favors the NLO properties and birefringence [14]. Therefore, in the recent years, searching for novel NLO materials able to produce coherent radiation in UV and DVU regions attracted many researchers. Good examples are $KBe_2BO_3F_2$ (KBBF) and $Sr_2Be_2B_2O_7$ (SBBO) single crystals [15–17] which can generate SHG in DUV region but due to the high toxicity of the beryllium oxide powders, it remains challenging to safely grow crystals of large size.

To overcome the high toxicity drawback, the substitution of Zn for Be is suggested to eliminate the toxicity components inherent in synthesis of KBBF and SBBO from beryllium oxide powder. Therefore, the discovery of new $CsZn_2B_3O_7$ crystal opens the way to safe crystal growth and increase the efficiency of the SHG almost to double in borates crystals due to the presence of the distorted $(ZnO_4)^{6-}$ tetrahedral. Moreover, the introduction of Zn atoms causes red-shift of the $CsZn_2B_3O_7$ absorption edge to 218 nm [13]. Therefore, we addressed ourselves to investigate the influence of

* New Technologies - Research Centre, University of West Bohemia, Univerzitni 8, 306 14 Pilsen, Czech Republic
E-mail address: maalidph@yahoo.co.uk.

http://dx.doi.org/10.1016/j.jallcom.2017.06.126
0925-8388/© 2017 Elsevier B.V. All rights reserved.

$(ZnO_4)^{6-}$ tetrahedra on the crystal structure, and hence, on the resulting SHG. We should emphasize that the reported SHG levels in $CsZn_2B_3O_7$ [15,18] are measured for a powder without taking into account the influence of the structural units packing. It is important to mention that, on the basis of anionic group theory [19], the overall SHG response of a crystal is the geometrical superposition of the second-order susceptibilities. Therefore, the packing of the BO_3 structural unit may also affect the macroscopic SHG coefficients [20]. The large SHG is due to hyperpolarizablity formed by the cations and co-parallel BO_3 triangle groups [20]. Therefore, this work is aimed at the qualitative and quantitative investigation to report the reliable SHG values and the details of the NLO tensor for $CsZn_2B_3O_7$ single crystal.

2. Methodology

The optical and physical properties of the newly synthesized $CsZn_2B_3O_7$ with sixteen formula per unit cell, space group $Cmc2_1$, were investigated [15,18]. $CsZn_2B_3O_7$ is isostructural to $KBe_2BO_3F_2$ (KBBF) [16,17], $Sr_2Be_2B_2O_7$ (SBBO) [21–24] and $KBe_2B_3O_7$, but it possesses larger SHG response due to the presence of the distorted $(ZnO_4)^{6-}$ tetrahedral. The $CsZn_2B_3O_7$ borate eliminates the toxicity issues from beryllium oxide powders and shows the red-shift of the absorption edge. To perform accurate calculation, the experimental X-ray diffraction data of $CsZn_2B_3O_7$ [18] are optimized utilizing the all-electron full-potential method (wien2k code [26]) within the generalized gradient approximation (PBE-GGA) [27]. The resulting optimized geometrical structure is used to calculate the ground state properties using the recently modified Becke-Johnson potential (mBJ) [28]. The crystal structure of $CsZn_2B_3O_7$ is shown in Fig. 1. In this calculation, the basis functions in the interstitial region are expanded up to $R_{MT} \times K_{max} = 7.0$ and inside the atomic spheres for the wave function. The $\boldsymbol{l}_{max} = 10$ and the charge density is Fourier expanded up to $G_{max} = 12$ $(a.u.)^{-1}$. To obtain the self-consistency, a mesh of 4000 $\vec{k}$ points in the irreducible Brillouin zone (IBZ) is used. The self-consistent calculations are converged since the total energy of the system is stable within 0.00001 Ry. A mesh of 50000 $\vec{k}$ points in the IBZ is used to perform the calculation of the linear and NLO properties. The inputs required for calculating the linear and NLO properties are the energy eigenvalues and eigenfunctions which are the natural outputs of band structure calculation. The linear optical properties are calculated using the optical code implemented in the Wien2k package [26]; for more details we refer readers to the users' guide [29] and [30]. The formalism for calculating the nonlinear optical properties is given elsewhere [31–34].

It is well known that the DFT approaches have the ability to accurately predict the ground state properties of the materials, and the developed analytical tools are vital to investigate their intrinsic mechanism. This microscopic understanding has further guided molecular engineering design for new crystals with novel structures and properties. It is anticipated that first-principle material approaches will greatly improve the search efficiency and greatly help experiments to save resources in the exploration of new crystals with good performance [35–44]. For instance, several researchers have used the DFT calculation for exploration the linear and nonlinear optical properties of new NLO material and found good agreement with the experimental results. We would like to mention here that, in our previous works [45–48], we have calculated the linear and nonlinear optical properties using FPLAPW method for several systems whose the linear and nonlinear optical susceptibility dispersion are known experimentally and a very good agreement with the experimental data was obtained. Thus, we believe that our calculations reported in this paper would produce very accurate and reliable results.

3. Obtained results and discussion

To confirm that a red-shift to 218 nm occurs in the absorption edge of $CsZn_2B_3O_7$ [13] with respect to the absorption edge of $KBe_2BO_3F_2$, $Sr_2Be_2B_2O_7$ and $KBe_2B_3O_7$ single crystals (144 nm) [16,17,21–25], the absorption spectra is calculated, as presented in Fig. 2 (a). The absorption edge's value of the semiconductor materials could be solved as follow; the square of absorption coefficient $I(\omega)$ is linear with energy (E) for direct optical transitions in the absorption edge region, whereas the square root of $I(\omega)$ is linear with E for indirect optical transitions [49,50]. Since the calculated electronic band structure of $CsZn_2B_3O_7$ (right inset in Fig. 2a) confirms the direct nature of the band gap, the data plots of the $[I(\omega)]^2$ versus E are shown in the left inset of Fig. 2a. It is evident that the $[I(\omega)]^2$ versus E is linear in the absorption edge region. These plots suggest that the absorption edge of the $CsZn_2B_3O_7$ is caused by direct transitions. Following Fig. 2a, we can conclude that the absorption edges of $CsZn_2B_3O_7$ occurs at $\lambda = 218$ nm and the optical band gap is estimated to be 5.68 eV in good agreement with the experimental data (5.69 eV) [18]. This finding motivated us to demonstrate the calculated imaginary and real parts of the optical dielectric function (Fig. 2b). The imaginary part show the first critical points (the absorption edges) for the three tensor components $\varepsilon_2^{xx}(\omega)$, $\varepsilon_2^{yy}(\omega)$ and $\varepsilon_2^{zz}(\omega)$ along the fundamental crystal axes, are located at 5.68 eV and the fundamental peaks occurs at 12.0, 9.0 and 10.0 eV for $\varepsilon_2^{xx}(\omega)$, $\varepsilon_2^{yy}(\omega)$ and $\varepsilon_2^{zz}(\omega)$, respectively. The calculated vanishing frequency value (static electronic dielectric constant $\varepsilon_\infty = \varepsilon_1(0)$) of the real part of the optical dielectric function confirms the occurrence of absorption edges at 5.68 eV since the calculated $\varepsilon_\infty = \varepsilon_1(0)$ is inversely related to the energy gap; this can be explained on the basis of the Penn model $\varepsilon_1(0) \approx 1 + (\hbar\omega_P/E_{optical\ gap})^2$ [51], where the calculated $\varepsilon_1(0)$ and the plasma energy $\hbar\omega_p$ for $CsZn_2B_3O_7$ are 1.5 and 4.023 eV, respectively. Thus, the $E_{optical\ gap}$ is about 5.68 eV and $\lambda = 1239.8/E_{optical\ gap} = 218$ nm. Therefore, the calculate imaginary and real parts of the optical dielectric function supports our finding that the absorption edge of $CsZn_2B_3O_7$ occurs at $\lambda = 218$ nm and the optical band gap is estimated to be 5.68 eV in good agreement with the experimental data (5.69 eV) [18]. Furthermore, the calculated refractive indices (Fig. 2c) confirm the value of $n(0) = \sqrt{\varepsilon_1(0)}$, Fig. 2c shows that the $n^{average}(0)$ occurs at 1.225 thus $\varepsilon_1^{average}(0) = 1.5$, and hence, the absorption edges of $CsZn_2B_3O_7$ occurs at $\lambda = 218$ nm. The calculated refractive indices at $\lambda = 218$ nm (5.68 eV) are shown in Table 1 and they are small enough to match the fundamental wave with the SHG light. From the calculated refractive indices, the birefringence can be obtained following $\Delta n(\omega) = n_e(\omega) - n_0(\omega)$, see Fig. 2d. The obtained values of the birefringence at the static limit and at $\lambda = 218$ nm are given in Table 1. Birefringence is important in fulfilling the phase-matching conditions. The calculated linear optical susceptibility dispersion show a considerable anisotropy, that favors an important quantity in SHG and OPO due to better fulfilling of phase-matching conditions determined by birefringence. Therefore, the calculated uniaxial anisotropy $\delta\varepsilon = [(\varepsilon_0^{II} - \varepsilon_0^{\perp})/\varepsilon_0^{tot}]$ [52] is about 0.047 which confirm the considerable anisotropy, and hence, the appropriate birefringence which is about 0.028, 0.029 and 0.051 at the static limit, $\lambda = 1064$ nm and at $\lambda = 218$ nm, respectively. Further investigation to the linear optical susceptibility dispersion, the reflectivity spectra and the loss function are calculated. The reflectivity spectra (Fig. 2e) show the first minimum at the plasma

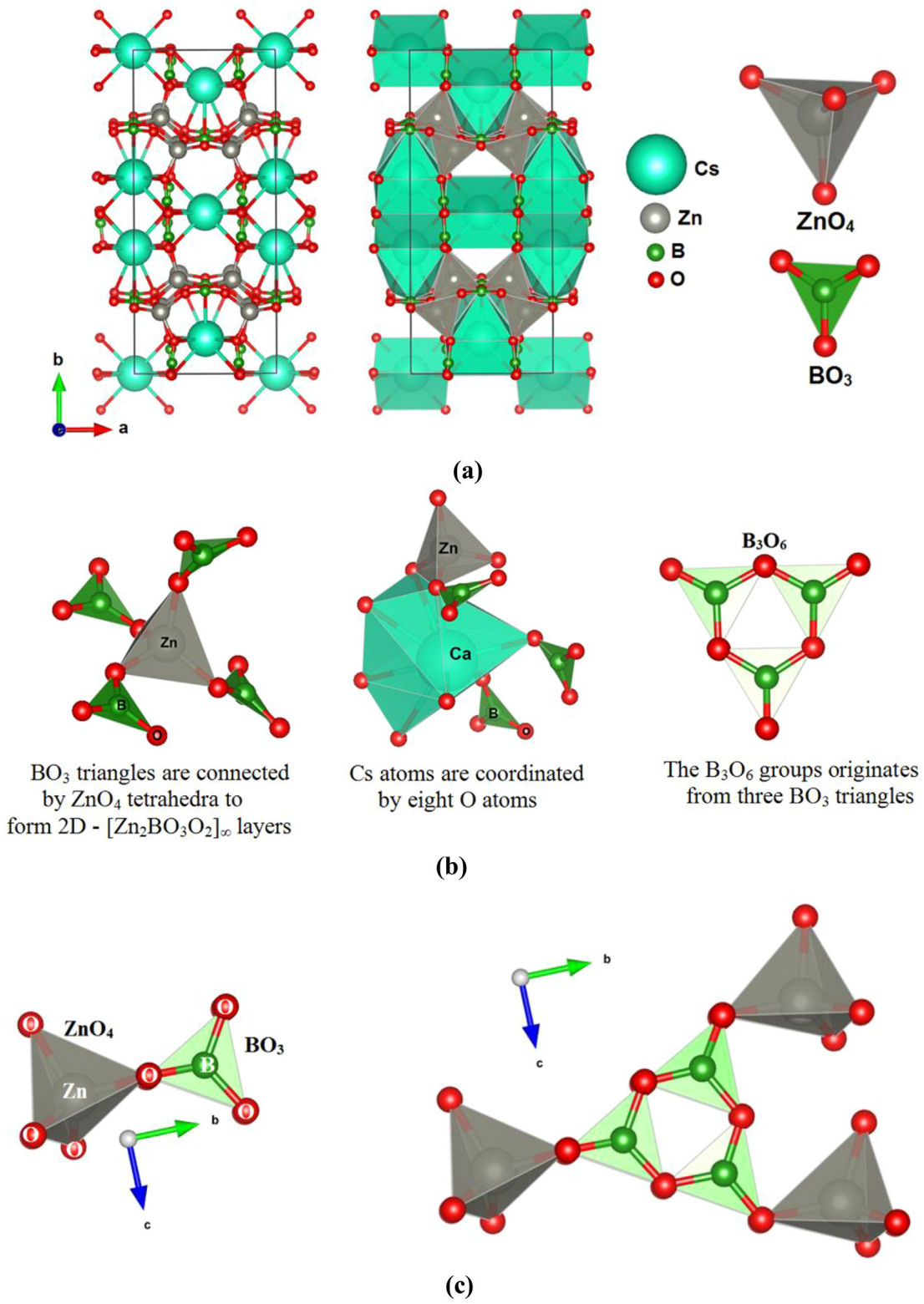

Fig. 1. (a, b) The crystal structure of the newly synthesized $CsZn_2B_3O_7$ in Cmc21 orthorhombic space group. B atoms are coordinated to three oxygen atoms to form planar BO_3 triangles. The BO_3 anionic groups exhibit planar shape with conjugated electron orbitals which make the BO_3 anionic groups is the main source of the large birefringence in $CsZn_2B_3O_7$. The distorted $(ZnO_4)^{6-}$ tetrahedra is the main source to increase the efficiency of the SHG. The crystal structure consists of $[Zn_2BO_3O_2]_\infty$ layers with adjacent layers connected by B_3O_6 groups. The B_3O_6 groups originates from the connection of three BO_3 triangles, in which only B3, B4 and B5 atoms are participated in B_3O_6 groups. Whereas B1, B2 and B6 atoms forms ($B1O_3$, $B2O_3$ and $B6O_3$) isolated triangles. These isolated triangles adopt a nearly coplanar configuration, which enhance the SHG and the birefringence in borate crystals.

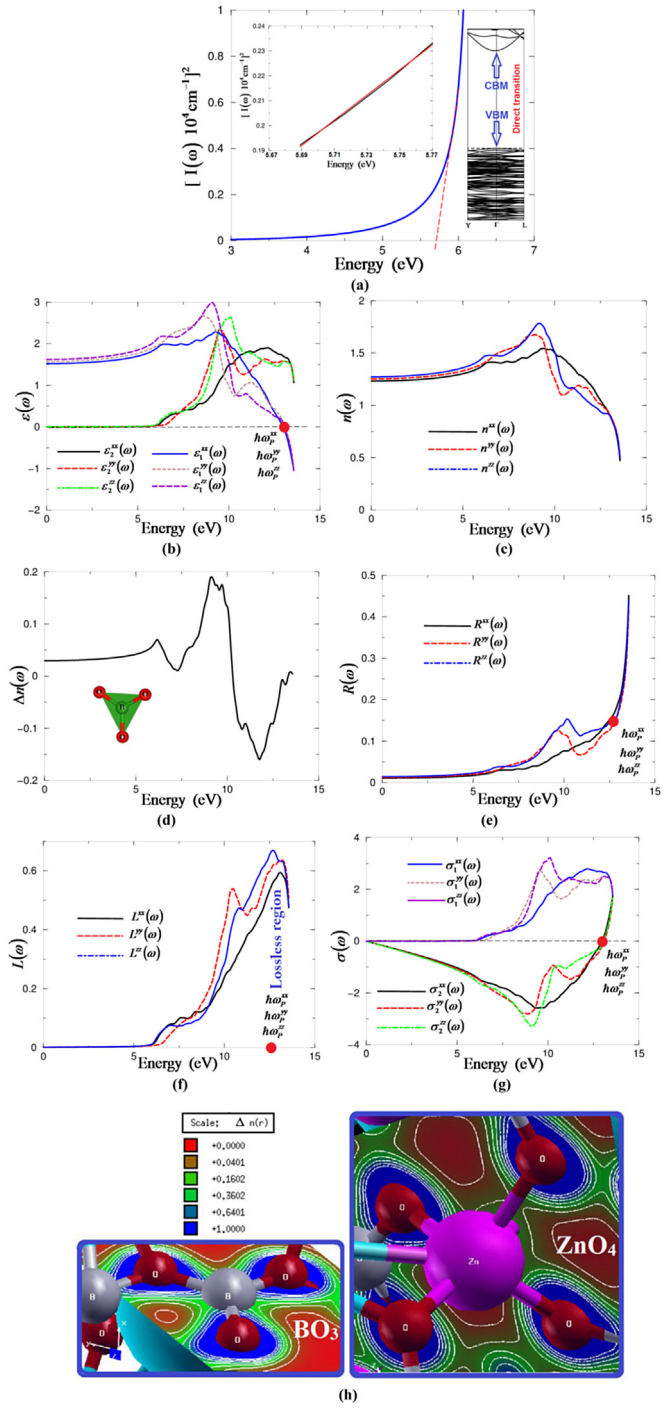

Fig. 2. **(a)** The calculated absorption spectra, since the calculated electronic band structure of $CsZn_2B_3O_7$ (right inset) confirms the indirect nature of the band gap therefore, data plots of the $[I(\omega)]^2$ versus E as shown in the left inset. It is clearly show that the $[I(\omega)]^2$ versus E is linear in the absorption edge region. These plots suggest that the absorption edge of the $CsZn_2B_3O_7$ is caused by direct transitions. Thus, we can conclude that the absorption edges of $CsZn_2B_3O_7$ occurs at $\lambda = 218$ nm and the optical band gaps are estimated to be 5.68 eV in good agreement with the experimental data (5.69 eV); **(b)** Calculated $\varepsilon_2^{xx}(\omega)$ (dark solid curve-black color online), $\varepsilon_2^{yy}(\omega)$ (light long dashed curve-red color online) and $\varepsilon_2^{zz}(\omega)$ (light dotted dashed curve -green color online) along with Calculated $\varepsilon_1^{xx}(\omega)$ (dark solid curve-blue color online), $\varepsilon_1^{yy}(\omega)$ (light dashed curve-brown color online) and $\varepsilon_1^{zz}(\omega)$ (light sold curve -violet color online); **(c)** Calculated refractive indices $n^{xx}(\omega)$ (dark solid curve-black color online), $n^{yy}(\omega)$ (light dashed curve-red color online) and $n^{zz}(\omega)$ (light dotted dashed curve -blue color online) spectrum; **(d)** Calculated birefringence $\Delta n(\omega)$; **(e)** Calculated $R^{xx}(\omega)$ (dark solid curve-black color online), $R^{yy}(\omega)$ (light dashed curve-red color online), and $R^{zz}(\omega)$ (light dotted dashed curve -blue color online); **(f)** Calculated loss function $L^{xx}(\omega)$ (dark solid curve-back color online), $L^{yy}(\omega)$ (light dashed curve-red color online) and $L^{zz}(\omega)$ (light dotted dashed curve -blue color online) spectrum; **(g)** Calculated $\sigma_2^{xx}(\omega)$ (dark solid curve-black color online), $\sigma_2^{yy}(\omega)$ (light dashed curve-red color online) and $\sigma_2^{zz}(\omega)$ (light dotted dashed curve -green color online) along with Calculated $\sigma_1^{xx}(\omega)$ (dark solid curve-blue color online), $\sigma_1^{yy}(\omega)$ (light dashed curve-red brown online) and $\sigma_1^{zz}(\omega)$ (light solid curve - violet color online); **(h)** The electron cloud of the BO_3 anionic groups which exhibit planar shape with conjugated electron orbitals which make the BO_3 anionic groups are the main source of the large birefringence in $CsZn_2B_3O_7$. The electron cloud of the distorted $(ZnO_4)^{6-}$ tetrahedra. (For interpretation of the references to colour in this figure legend, the reader is referred to the web version of this article.)

frequency (i.e. 12.5 eV) the energy point where optical spectra of $\varepsilon_1^{xx}(\omega)$, $\varepsilon_1^{yy}(\omega)$, $\varepsilon_1^{zz}(\omega)$ cross zero, confirming the occurrence of a collective plasmon resonance in concordance with our observation in Fig. 2b.

The loss function's peaks (Fig. 2f), are initiated at the values of the plasma frequencies ω_p^{xx} , ω_p^{yy} and ω_p^{zz} at the energy point where optical spectra of $\varepsilon_1^{xx}(\omega)$, $\varepsilon_1^{yy}(\omega)$, $\varepsilon_1^{zz}(\omega)$ cross zero. The frequency-dependent optical conductivity (Fig. 2g) can be obtained from the complex first-order linear optical dielectric function following the expression $\varepsilon(\omega) = \varepsilon_1(\omega) + i\varepsilon_2(\omega) = 1 + \frac{4\pi i\sigma(\omega)}{\omega}$, [53,54]. It consists of imaginary and real parts; therefore, it completely characterizes the linear optical properties. The imaginary part $\sigma_2^{xx}(\omega)$, $\sigma_2^{yy}(\omega)$ and $\sigma_2^{zz}(\omega)$ between 0.0 and the values of ω_p^{xx} , ω_p^{yy} and ω_p^{zz} exhibit overturned features of $\varepsilon_2^{xx}(\omega)$, $\varepsilon_2^{yy}(\omega)$ and $\varepsilon_2^{zz}(\omega)$, whereas the real parts $\sigma_1^{xx}(\omega)$, $\sigma_1^{yy}(\omega)$ and $\sigma_1^{zz}(\omega)$ show similar features to those of $\varepsilon_2^{xx}(\omega)$, $\varepsilon_2^{yy}(\omega)$ and $\varepsilon_2^{zz}(\omega)$. The intersection of the imaginary and real parts of the optical conductivity at the zero energy represents the values of ω_p^{xx} , ω_p^{yy} and ω_p^{zz}.

KBBF derivatives contain two types of B−O groups and one of B−O group consists of the coparallel BO_3 triangles. The second B−O group is located between the two adjacent $[Be_2BO_3O_2]$ and connecting them together with antiparallel arrangement, resulting in canceling their contribution to the macroscopic SHG response. Hence, the SHG responses in KBBF derivatives mainly arise from the coparallel BO_3 triangles. Therefore, the number density of the coparallel BO_3 triangles will determine the SHG response of the KBBF structures [46,55]. While in $CsZn_2B_3O_7$, the B_3O_6 groups are located between adjacent $[Zn_2BO_3O_2]$ layers and they are anti-aligned (Fig. 1c). Thus, the SHG response of $CsZn_2B_3O_7$ should also come from the coparallel BO_3 triangles, which was confirmed by Yu et. al. [15]. They reported the net dipole moment of the BO_3 triangles and $(ZnO_4)^{6-}$ tetrahedra are pointed along the polar c-axis which means that BO_3 triangles and $(ZnO_4)^{6-}$ tetrahedra contributions to the SHG response are larger than that of B_3O_6 groups [15]. Moreover, our investigation confirm that the $CsZn_2B_3O_7$ possesses large birefringence, considerable anisotropy in the linear optical properties, the absorption edge occurs at $\lambda = 218$ nm and the presence of the distorted $(ZnO_4)^{6-}$ tetrahedra. This opens the way to safely grown NLO crystals and the twice increase of the SHG efficiency occurs in reference to other borates crystals in the DVU region. Therefore, based on these promising results, we calculated the nonlinear optical susceptibility dispersion of $CsZn_2B_3O_7$ single crystal. Due to the symmetry, the $CsZn_2B_3O_7$ single crystal possesses five non-zero tensor components and one of them exhibit the dominant contribution. The calculated five tensor components are shown in Fig. 3a. It is clear that the 333 tensor component is dominant at the static limit and at $\lambda = 1064$ nm. The calculated value of the dominant tensor component $\left|\chi_{333}^{(2)}(\omega)\right|$ is about 1.17 p.m./V at static limit and 1.19 p.m./V at $\lambda = 1064$ nm, and, therefore, $d_{33} = 0.585$ p.m./V and 0.595 p.m./V at static limit and at $\lambda = 1064$ nm, respectively. The calculated value is in good

Table 1
The calculated energy band gap in comparison with the experimental value, $\varepsilon_1^{xx}(0)$, $\varepsilon_1^{yy}(0)$, $\varepsilon_1^{zz}(0)$, $\delta\varepsilon$, ω_p^{xx}, ω_p^{yy}, ω_p^{zz}, $n^{xx}(0)$, $n^{yy}(0)$, $n^{zz}(0)$, $\Delta n(0)$, $\Delta n(\omega)$.

	$CsZn_2B_3O_7$	
	This work	**Exp.**
Eg (eV)	5.68	5.69 [a]
$\varepsilon_1^{xx}(0)$	1.520	
$\varepsilon_1^{yy}(0)$	1.571	
$\varepsilon_1^{zz}(0)$	1.620	
$\delta\varepsilon$	0.047	
ω_p^{xx}	12.966	
ω_p^{yy}	13.102	
ω_p^{zz}	13.047	
$n^{xx}(0)$	1.233 1.341 at λ =218 nm	
$n^{yy}(0)$	1.253 1.368 at λ =218 nm	
$n^{zz}(0)$	1.273 1.404 at λ =218 nm	
$\Delta n(0)$	0.028	
$\Delta n(\omega)$ at λ =1064 nm	0.029	
$\Delta n(\omega)$ at λ =218 nm	0.051	

[a]Ref. 18 (experimental work)

agreement with the measure one 1.5 × KDP (1.5 × 0.39 p.m./V = 0.585 p.m./V) [18]. The values of the other tensor components are calculated and presented in Table 2. Further, we calculated the imaginary and real parts of the dominant tensor component i. e $\chi^{(2)}_{333}(\omega)$, as shown in Fig. 3b. It is shown that the highest intensity is around half value of the optical band gap (i.e. 2.84 eV) which is mainly formed by the 2ω resonance, while above the half value of the optical band gap the contribution comes from both 2ω and ω. To explain this, we have analyzed the spectral features of $\left|\chi^{(2)}_{333}(\omega)\right|$. A step forward, the absorptive part of the corresponding dielectric function $\varepsilon_2(\omega)$ as a function of both $\omega/2$ and ω is associated with spectral structures of $\left|\chi^{(2)}_{333}(\omega)\right|$, as shown in Fig. 2c. For simplicity, the spectral structures of $\varepsilon_2(\omega)$, $\varepsilon_2(\omega/2)$ and $\left|\chi^{(2)}_{333}(\omega)\right|$ can be divided into three spectral regions. The spectral region confined between $E_g/2$ and E_g is mainly formed by the 2ω resonance, which is associated with the main spectral structure of $\varepsilon_2(\omega/2)$. The second structure between E_g and 7.5 eV is associated with interference between 2ω andω resonances, which is associated with the first spectral structure of $\varepsilon_2(\omega)$. It is clear that in this region the ω terms start to oscillate and contribute to the spectral structure of $\left|\chi^{(2)}_{333}(\omega)\right|$ in addition to 2ω terms. The third spectral structure from 7.5 eV to 13.5 eV is mainly due to ω resonance which is associated with the second structure in $\varepsilon_2(\omega)$.

The imaginary and real parts are further separated into $2\omega/\omega$

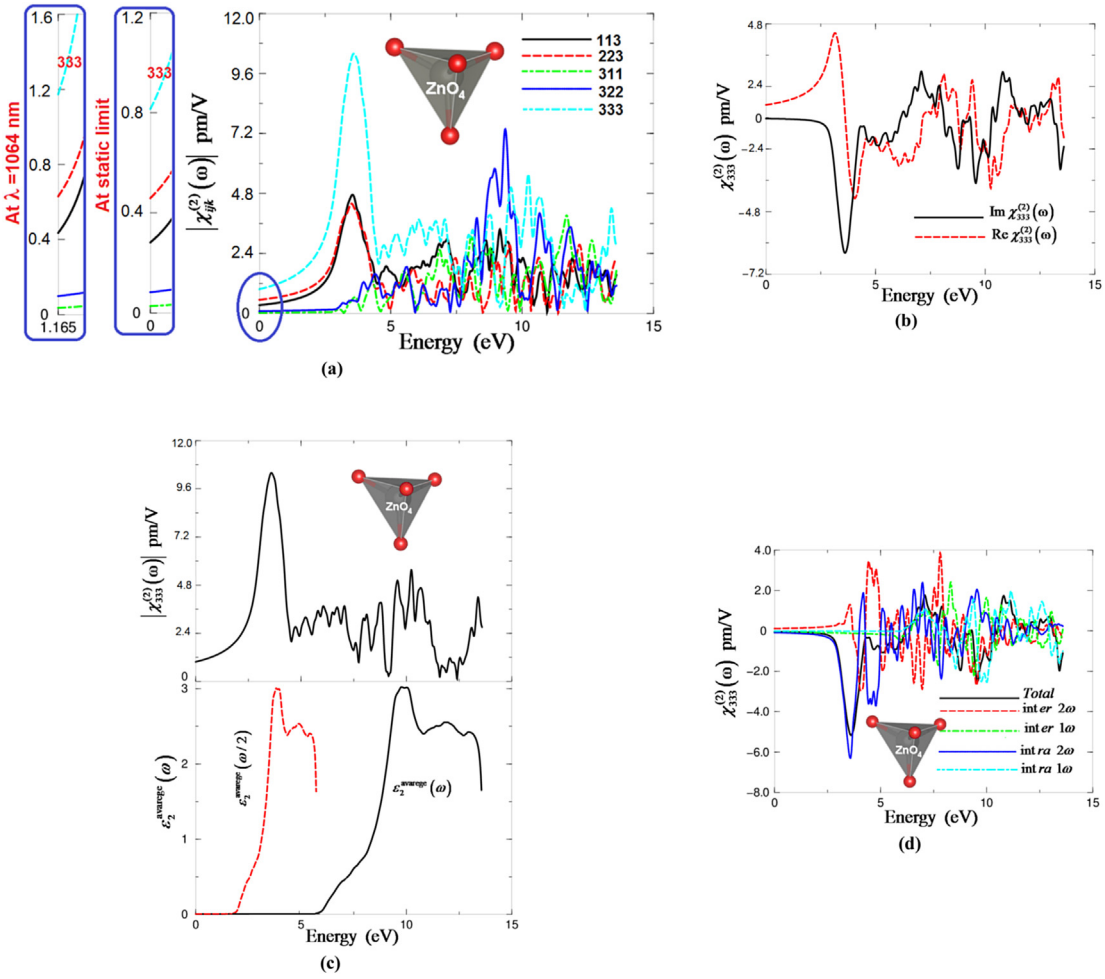

Fig. 3. **(a)** Calculated $\left|\chi^{(2)}_{ijk}(\omega)\right|$ for the five tensor components of $CsZn_2B_3O_7$; **(b)** Calculated Imaginary $\chi^{(2)}_{333}(\omega)$ (**dark solid curve-black color online**) and real $\chi^{(2)}_{333}(\omega)$ (light dashed curve-red color online) spectra; **(c)** –***upper panel***- Calculated $\left|\chi^{(2)}_{333}(\omega)\right|$ (dark solid curve-black color online); -***lower panel***- Calculated $\varepsilon^{xx}_2(\omega)$ (**dark solid curve-black color online**); Calculated $\varepsilon^{xx}_2(\omega/2)$ (**dark dashed curve-red color online**); **(d)** Calculated total $\mathrm{Im}\chi^{(2)}_{333}(\omega)$ spectrum (**dark solid curve-black color online**) along with the intra $(2\omega)/(1\omega)$ (light solid curve-blue color online)/(light dashed doted curve-cyan color online) and inter $(2\omega)/(1\omega)$ (light long dashed curve-red color online)/(light doted curve-green color online) -band contributions. (For interpretation of the references to colour in this figure legend, the reader is referred to the web version of this article.)

Table 2
Calculated $\left|\chi^{(2)}_{ijk}(\omega)\right|$ and β_{ijk} $CsZn_2B_3O_7$, in pm/V at static limit and at $\lambda = 1064$ nm.

$CsZn_2B_3O_7$				
Tensor components	$\chi^{(2)}_{ijk}(0)$	Theory $d_{ijk} = 0.5\chi^{(2)}_{ijk}(\omega)$ at static limit	$\chi^{(2)}_{ijk}(\omega)$ at $\lambda = 1064$ nm	Theory $d_{ijk} = 0.5\chi^{(2)}_{ijk}(\omega)$ $\lambda = 1064$ nm
$\left\|\chi^{(2)}_{113}(\omega)\right\|$	0.4014	d_{15}=0.2007	0.4382	d_{15}=0.2191
$\left\|\chi^{(2)}_{223}(\omega)\right\|$	0.6308	d_{14}=0.3154	0.6352	d_{14}=0.3176
$\left\|\chi^{(2)}_{311}(\omega)\right\|$	0.0401	d_{11}=0.0200	0.0402	d_{11}=0.0201
$\left\|\chi^{(2)}_{322}(\omega)\right\|$	0.1204	d_{12}=0.0602	0.0964	d_{12}=0.0482
$\left\|\chi^{(2)}_{333}(\omega)\right\|$	**1.1710**	***d*$_{33}$=0.5855**	**1.1910**	***d*$_{33}$=0.5955**
β_{333}	**0.2505 × 10^{-30} esu**		**0.2548 × 10^{-30} esu**	

The bold are the values of the dominate components.

inter-/intra-band contributions. Fig. 2d illustrate the $2\omega/\omega$ inter-/intra-band contributions of the imaginary part of $\chi^{(2)}_{333}(\omega)$. It is clear that the $2\omega/\omega$ inter-/intra-band contributions oscillate around zero and exhibit a considerable anisotropy. The sum of those contributions gives the total value of the imaginary part of the SHG.

Further, we have obtained the values of the microscopic first hyperpolarizability, β_{ijk} [56], the vector component along the dipole moment direction, at the static limit and at $\lambda = 1064$ nm. We should emphaize that the β_{ijk} term cumulatively yield a bulk observable second order susceptibility term, $\chi^{(2)}_{ijk}(\omega)$, which in turn is responsible for the strong SHG response [57]. Since $\chi^{(2)}_{333}(\omega)$ is the dominant component at the static limit and at $\lambda = 1064$ nm, we have presented in Table 2 the values of β_{333} at the static limit and at

the wavelength 1064 nm.

4. Conclusions

An ab-initio calculation utilizing the full-potential method is used to investigate the linear and nonlinear optical susceptibility dispersion of $CsZn_2B_3O_7$ single crystal of the bulk structure in form of single crystal, taking into account the influence of the packing structural units. We found that the packing of the BO_3 structural unit is the main source for the large birefringence, and hence, affect the macroscopic SHG coefficients. The large SHG is due to hyper-polarizablity formed by ZnO_4 tetrahedra and co-parallel BO_3 tri-angle groups. The accuracy of mBJ approach helps to accommodated the absorption edge of $CsZn_2B_3O_7$ occurs at $\lambda = 218$ nm and the optical band gap is estimated to be 5.68 eV in good agreement with the experimental data (5.69 eV) therefore, $CsZn_2B_3O_7$ is expected to produce a laser radiation in DUV region. The resulting SHG is 1.5 times of the well-known NLO crystal KDP, in good agreement with the measured value.

Acknowledgments

The result was developed within the CENTEM project, reg. no. CZ.1.05/2.1.00/03.0088, cofunded by the ERDF as part of the Ministry of Education, Youth and Sports OP RDI programme and, in the follow-up sustainability stage, supported through CENTEM PLUS (LO1402) by financial means from the Ministry of Education, Youth and Sports under the National Sustainability Programme I. Computational resources were provided by MetaCentrum (LM2010005) and CERIT-SC (CZ.1.05/3.2.00/08.0144) infrastructures.

References

[1] P.A. Franken, G. Weinreich, C.W. Peters, A.E. Hill, Generation of optical harmonics, Phys. Rev. Lett. 7 (1961) 118.
[2] Y.M. Xu, Y.B. Huang, X.Y. Cui, E. Razzoli, M. Radovic, M. Shi, G.F. Chen, P. Zheng, N.L. Wang, C.L. Zhang, et al., Nat. Phys. 7 (2011) 198–202.
[3] S. Neil, Ultraviolet lasers, Nat. Phot. 1 (2007) 83–85.
[4] D.M. Burland, R.D. Miller, C.A. Walsh, Second-order nonlinearity in poled-polymer systems, Chem. Rev. 94 (1994) 31–75.
[5] J. Chiaverini, D. Leibfried, T. Schaetz, M.D. Barrett, R.B. Blakestad, J. Britton, W.M. Itano, J.D. Jost, E. Knill, C. Langer, et al., Nonlinear optics in the extreme ultraviolet, Nature 432 (2004) 605–608.
[6] T. Kiss, F. Kanetaka, T. Yokoya, T. Shimojima, K. Kanai, S. Shin, Y. Onuki, T. Togashi, C. Zhang, C.T. Chen, et al., Phys. Rev. Lett. 94 (2005) 057001.
[7] L.P. Yatsenko, B.W. Shore, T. Halfmann, K. Bergmann, Phys. Rev. A 94 (1999) R4237.
[8] T. Kiss, T. Shimojima, T. Kanaia, T. Yokoya, S. Shin, Y. Onuki, T. Togashi, C. Zhang, C.T. Chen, J. Electron Spectrosc. 144 (2005) 953–956.
[9] J. Meng, G. Liu, W. Zhang, L. Zhao, H. Liu, X. Jia, D. Mu, S. Liu, X. Dong, J. Zhang, et al., Nature 462 (2009) 335–338.
[10] G. Balakrishnan, Y. Hu, S.B. Nielsen, T.G. Spiro, Appl. Spectrosc. 59 (2005) 776–781.
[11] P. Becker, Borate materials in nonlinear optics, Adv. Mater. 10 (1998) 979–992.
[12] X. Jiang, S. Luo, L. Kang, P. Gong, H. Huang, S. Wang, Z. Lin, C. Chen, ACS Photonics 2 (2015) 1183–1191.
[13] Yi Yang, Xingxing Jiang, Zheshuai Lin, Yicheng Wu, Crystals 7 (2017) 95, http://dx.doi.org/10.3390/cryst7040095.
[14] C.T. Chen, T. Sasaki, R. Li, Y. Wu, Z. Lin, Y. Mori, Z. Hu, J. Wang, G. Aka, M. Yoshimura, et al., Nonlinear Optical Borate Crystals Principals and Applications, Wiley-VCH, New York, NY, USA, 2012.
[15] H. Yu, H. Wu, S. Pan, Z. Yang, X. Hou, X. Su, Q. Jing, K.R. Poeppelmeier, J.M. Rondinelli, J. Am. Chem. Soc. 136 (2014) 1264–1267.
[16] C.T. Chen, J.H. Lu, T. Togashi, T. Suganuma, T. Sekikawa, S. Watanabe, Z.Y. Xu, J.Y. Wang, Opt. Lett. 27 (2002) 637.
[17] (a) B.C. Wu, D.Y. Tang, N. Ye, C.T. Chen, Opt. Mater. 5 (1996) 105; (b) C.T. Chen, G.L. Wang, X.Y. Wang, Z.Y. Xu, Appl. Phys. B Lasers Opt. 97 (2009) 9.
[18] S. Zhao, J. Zhang, S.Q. Zhang, Z. Sun, Z. Lin, Y. Wu, M. Hong, J. Luo, Inorg. Chem. 53 (2014) 2521–2527.
[19] (a) N. Ye, Q. Chen, B.C. Wu, C.T. Chen, J. Appl. Phys. 84 (1998) 555–558; (b) C. Chen, N. Ye, J. Lin, J. Jiang, W.R. Zeng, B.C. Wu, Adv. Mater. 11 (1999) 1071–1078.
[20] M. Abudoureheman, L. Wang, X. Zhang, H. Yu, Z. Yang, C. Lei, J. Han, S. Pan, Inorg. Chem. 54 (2015) 4138–4142.
[21] C.T. Chen, Y.B. Wang, B.C. Wu, K. Wu, W. Zeng, L.H. Yu, Nature 373 (1995) 322.
[22] H. Qi, C.T. Chen, Chem. Lett. 30 (2001) 354.
[23] N. Ye, W.R. Zeng, B.C. Wu, X.Y. Huang, C.T.Z. Chen, Kristallogr 213 (1998) 452.
[24] N. Ye, W.R. Zeng, J. Jiang, B.C. Wu, C.T. Chen, B.H. Feng, X.L. Zhang, J. Opt. Soc. Am. B 17 (2000) 764.
[25] S.C. Wang, N. Ye, W. Li, D.J. Zhao, Am. Chem. Soc. 132 (2010) 8779–8786.
[26] P. Blaha, K. Schwarz, G.K.H. Madsen, D. Kvasnicka, J. Luitz, WIEN2k, An Augmented Plane Wave Plus Local Orbitals Program for Calculating Crystal Properties, Vienna University of Technology, Austria, 2001.
[27] J.P. Perdew, S. Burke, M. Ernzerhof, Phys. Rev. Lett. 77 (1996) 3865.
[28] F. Tran, P. Blaha, Phys. Rev. Lett. 102 (2009) 226401.
[29] http://www.wien2k.at/reg_user/textbooks/usersguide.pdf.
[30] C. Ambrosch-Draxl, J.O. Sofo, Comput. Phys. Commun. 175 (2006) 1–14.
[31] S. Sharma, J.K. Dewhurst, C. Ambrosch-Draxl, Phys. Rev. B 67 (2003) 165332.
[32] Ph.D. thesis, A. H. Reshak, Indian Institute of Technology-Rookee, India (2005).
[33] A.H. Reshak, J. Chem. Phys. 125 (2006) 03471.
[34] A.H. Reshak, J. Chem. Phys. 124 (2006) 104707.
[35] Zheshuai Lin, Xingxing Jiang, Lei Kang, Pifu Gong, Siyang Luo, Ming-Hsien Lee, J. Phys. D. Appl. Phys. 47 (2014) 253001.
[36] M.I. Kolinko, I.V. Kityk, A.S. Krochuk, J. Phys. Chem. Solids 53 (1992) 1315–1320.
[37] G.E. Davydyuk, O.Y. Khyzhun, A.H. Reshak, H. Kamarudin, G.L. Myronchuk, S.P. Danylchuk, A.O. Fedorchuk, L.V. Piskach, M. Yu. Mozolyuk, O.V. Parasyuk, Phys. Chem. Chem. Phys. 15 (2013) 6965.
[38] A.H. Reshak, Y.M. Kogut, A.O. Fedorchuk, O.V. Zamuruyeva, G.L. Myronchuk, O.V. Parasyuk, H. Kamarudin, S. Auluck, K.L. Plucinskig, J. Bila, Phys. Chem. Chem. Phys. 15 (2013) 18979.
[39] V.V. Atuchin, T.A. Gavrilova, J.-C. Grivel, V.G. Kesler, Surf. Sci. 602 (2008) 3095–3099.
[40] V.V. Atuchin, T.A. Gavrilova, J.-C. Grivel, V.G. Kesler, J. Phys. D. Appl. Phys. 42 (2009) 035305.
[41] O.Y. Khyzhun, V.L. Bekenev, V.V. Atuchin, E.N. Galashov, V.N. Shlegel, Mater. Chem. Phys. 140 (2013) 558–595.
[42] V.V. Atuchin, E.N. Galashov, O.Y. Khyzhun, V.L. Bekenev, L.D. Pokrovsky, Yu.A. Borovlev, V.N. Zhdankov, J. Solid State Chem. 236 (2016) 24–31.
[43] Hongwei Huang, Xiaowei Li, Jinjian Wang, Fan Dong, Paul K. Chu, Tierui Zhang, Yihe Zhang, ACS Catal. 5 (7) (2015) 4094–4103.
[44] Hongwei Huang, Xu Han, Xiaowei Li, Shichao Wang, Paul K. Chu, Yihe Zhang, ACS Appl. Mater. Interfaces 7 (2015) 482–492.
[45] A. H. Reshak, Sci. Rep. 7 46415 http://dx.doi.org/10.1038/srep46415.
[46] A.H. Reshak, S. Auluck, RSC Adv. 7 (2017) 14752.
[47] A.H. Reshak, M.G. Brik, J. Alloys Compd. 675 (2016) 355–363.
[48] A.H. Reshak, J. Appl. Phys. 119 (2016) 105706.
[49] H. Huang, Y. He, X. Li, M. Li, C. Zeng, F. Dong, X. Du, T. Zhangd, Y. Zhang, J. Mater. Chem. A 3 (2015) 24547–24556.
[50] H. Huang, Y. He, Z. Lin, L. Kang, Y. Zhang, J. Phys. Chem. C 117 (2013) 22986–22994.
[51] D.R. Penn, Phys. Rev. B 128 (1962) 2093.
[52] G.D. Boyd, H. Kasper, J.H. McFee, IEEE J. Quantum Electron 7 (1971) 563.
[53] F. Bassani, G.P. Parravicini, Electronic States and Optical Transitions in Solids, Pergamon Press Ltd., Oxford, 1975, pp. p149–154.
[54] C. Ambrosch-Draxl, J.O. Sofo, Comput. Phys. Commun. 175 (2006) 1–14.
[55] C.T. Chen, Y.B. Wang, B.C. Wu, K. Wu, W. Zeng, L.H. Yu, Nature 373 (1995) 322.
[56] R.Y. Boyd, Principles of Nonlinear Optics, Academic Press, NY, 1982, p. 420.
[57] R.W. Boyd, Nonlinear Optics, third ed., Academic Press is an imprint of Elsevier, 2008. ISBN:978-0-12-369470-6.